

Numerical Dispersion in 3D Time-Domain Finite-Difference Wave Propagation Algorithms

SAND2005-7724C



Sandia
National
Laboratories

Matthew M. Haney, David F. Aldridge, and Neill P. Symons

Geophysics Department, Sandia National Laboratories, Albuquerque, New Mexico



Introduction

Numerical solution of partial differential equations by explicit, time-domain, finite-difference (FD) techniques entails approximating temporal and spatial derivatives by discrete function differences. Hence, the solution of the difference equation will not be identical to the solution of the underlying differential equation. Solution accuracy degrades if the grid intervals are too large. Overly coarse spatial gridding leads to spurious artifacts in the calculated results referred to as *numerical dispersion*, whereas coarse temporal sampling may produce *numerical instability* (manifest as unbounded growth in the calculations as FD timestepping proceeds). Quantitative conditions for minimizing dispersion and avoiding instability are developed by deriving the *dispersion relation* appropriate for the discrete difference equation (or coupled system of difference equations) under examination. In this study, a dispersion relation appropriate for 3D O(M,N) staggered-grid, FD solution of the velocity-stress elastodynamic system is derived, from which formulae for discrete phase speed, group speed, and particle velocity polarization are developed.

Velocity-Stress Elastodynamic System and Finite-Difference Grid

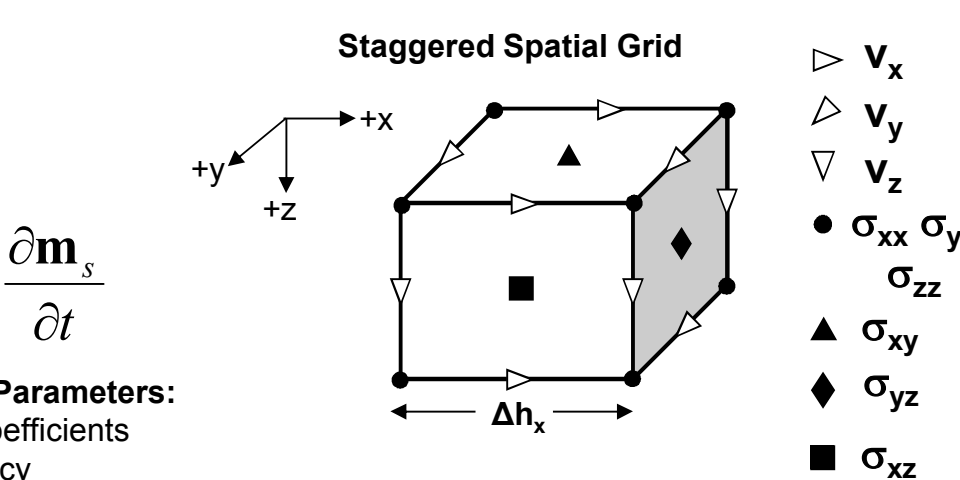
Nine, coupled, first-order, non-homogeneous, partial differential equations:

$$\frac{\partial \mathbf{v}}{\partial t} - b(\nabla \cdot \boldsymbol{\sigma}) = b(\mathbf{f} + \nabla \cdot \mathbf{m}_a)$$

$$\frac{\partial \boldsymbol{\sigma}}{\partial t} - \lambda(\nabla \cdot \mathbf{v})\mathbf{I} - \mu(\nabla \mathbf{v} + \nabla \mathbf{v}^T) = \frac{\partial \mathbf{m}}{\partial t}$$

Wavefield Variables: $\mathbf{v}(x,t)$ - velocity vector
 $\boldsymbol{\sigma}(x,t)$ - stress tensor

Elastic Earth Model Parameters: $\lambda(x)$, $\mu(x)$ - Lamé coefficients
 $b(x)$ - mass buoyancy



Seismic Body Sources:
 $\mathbf{f}(x,t)$ - force density vector
 $\mathbf{m}(x,t)$ - moment density tensor

Staggered Spatial Grid
 Δx
 Δt
 Δy
 Δz

3D velocity-stress system is numerically solved with an explicit, time-domain, O(2,4) staggered-grid, FD algorithm

O(2,N) Stability Factor, Phase & Group Speeds, and Polarization Measure

Derivational procedure is a modern variant of **von Neumann analysis**: assume a homogeneous wholespace with no body sources, and perform a 4D discrete space/time Fourier transform of coupled system of FD updating formulae. Numerical *dispersion relation* is obtained by setting determinant of matrix of coefficients in transformed (i.e., algebraic) system equal to zero. Further manipulation yields:

1) FD Stability Factor:

$$\eta = \sqrt{3} \left(\frac{c \Delta t}{\Delta h} \right)^{N/2} \sum_{n=1}^{N/2} |b_n|$$

b_n are coefficients of an O(N) staggered, spatial FD operator.
 Δt = FD timestep, Δh = spatial grid interval.

For FD algorithm stability, must have $\eta < 1$, where c is maximum wavespeed in 3D earth model!

2) Plane Wave Phase Speed:

$$\frac{c_{\text{phase}}(s, \theta, \phi)}{c} = \frac{\sqrt{3} \sum_{n=1}^{N/2} |b_n|}{\pi \eta s} \sin^{-1} \left[\frac{\eta K(s, \theta, \phi)}{\sqrt{3} \sum_{n=1}^{N/2} |b_n|} \right],$$

$s = \Delta h / \lambda$ = spatial sampling ratio.

(θ, ϕ) = polar and azimuthal propagation direction angles of a plane harmonic wave with wavelength λ .

where $K^2(s, \theta, \phi) = K_x^2 + K_y^2 + K_z^2 =$

$$\left[\sum_{n=1}^{N/2} b_n \sin[(2n-1)\pi s \sin \theta \cos \phi] \right]^2 + \left[\sum_{n=1}^{N/2} b_n \sin[(2n-1)\pi s \sin \theta \sin \phi] \right]^2 + \left[\sum_{n=1}^{N/2} b_n \sin[(2n-1)\pi s \cos \theta] \right]^2.$$

3) Plane Wave Group Speed:

$$\frac{c_{\text{group}}(s, \theta, \phi)}{c} = \frac{\partial}{\partial s} \left[\frac{c_{\text{phase}}(s, \theta, \phi)}{c} \right] - \text{obtained by differentiating phase speed.}$$

4) Particle Velocity Polarization:

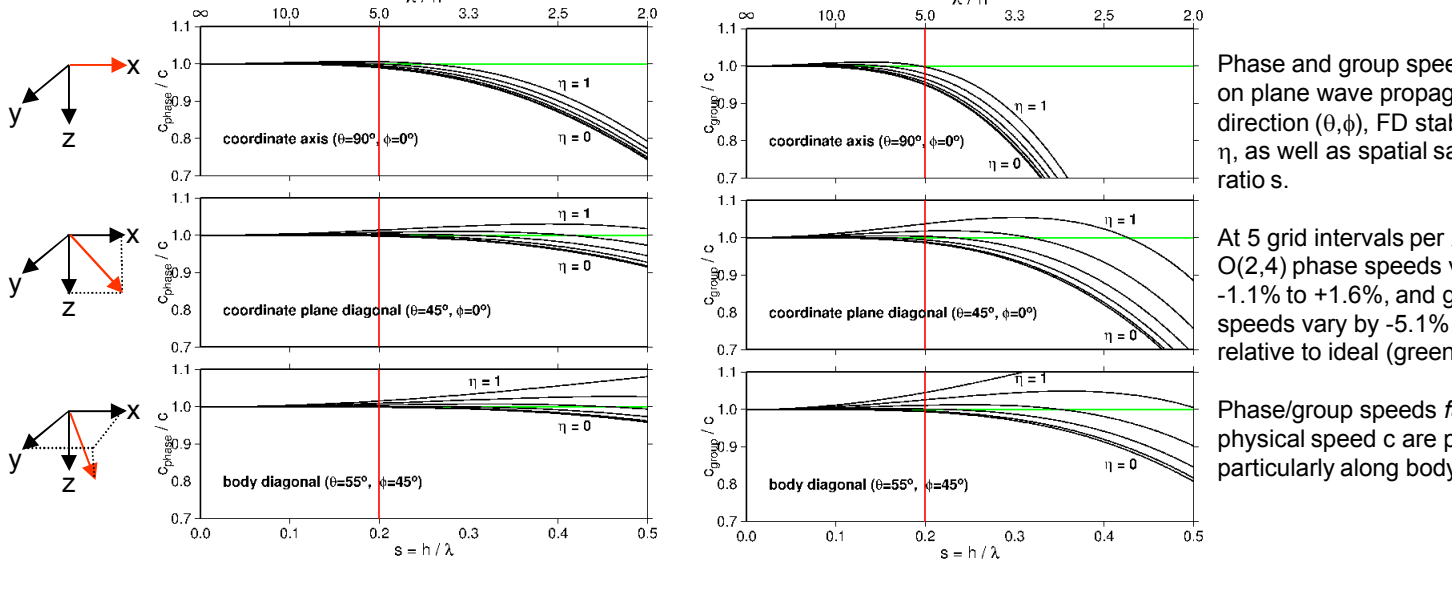
$$P(s, \theta, \phi) = \mathbf{n}(\theta, \phi) \cdot \frac{\mathbf{K}(s, \theta, \phi)}{\|\mathbf{K}\|} - \text{dot product of unit propagation direction vector } \mathbf{n} \text{ and normalized discrete wavenumber vector.}$$

NOTES:

- 1) Plane wave phase and group speed formulae, and polarization measure apply to either P-waves or S-waves.
- 2) All formulae reduce to analogous continuous expressions in limit of vanishing temporal and spatial grid intervals.
- 3) Generalization to unequal spatial grid intervals ($\Delta x \neq \Delta y \neq \Delta z$) exist.
- 4) 3D formulae reduce to appropriate 2D and 1D versions as one or two spatial grid intervals $\rightarrow \infty$, respectively.
- 5) Generalization to higher-order temporal FD operator ($M > 2$) exist.

Numerical Examples: Phase/Group Speed and Polarization

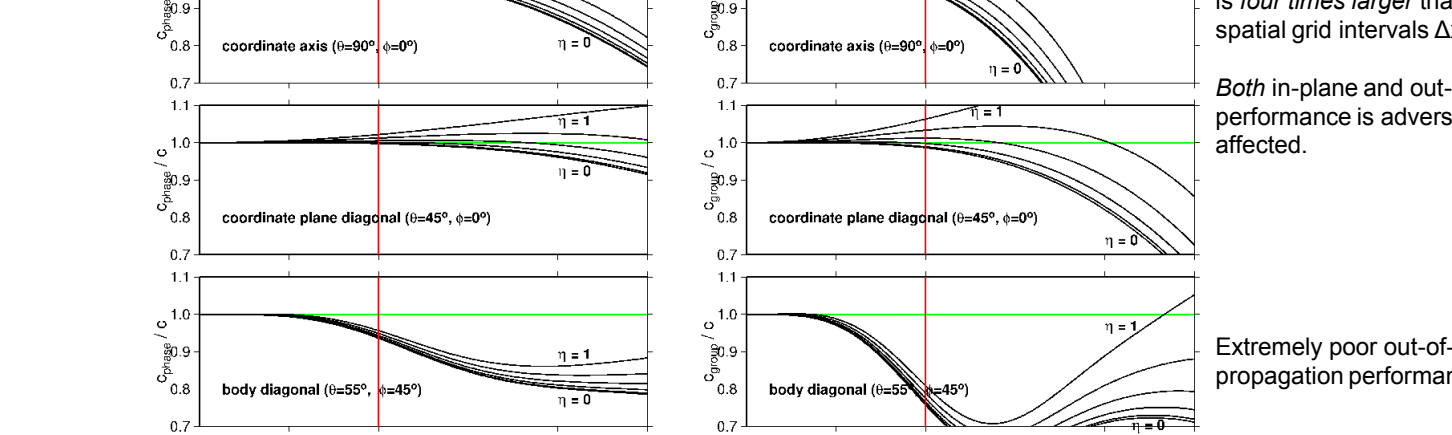
O(2,4) Phase Speed



At 5 grid intervals per λ , O(2,4) phase speeds vary by -1.1% to +4.5%, and group speeds vary by -1.1% to +4.5%, relative to ideal (green line).

Phase/group speeds faster than physical speed c are possible, particularly along body diagonal.

O(2,4) Group Speed

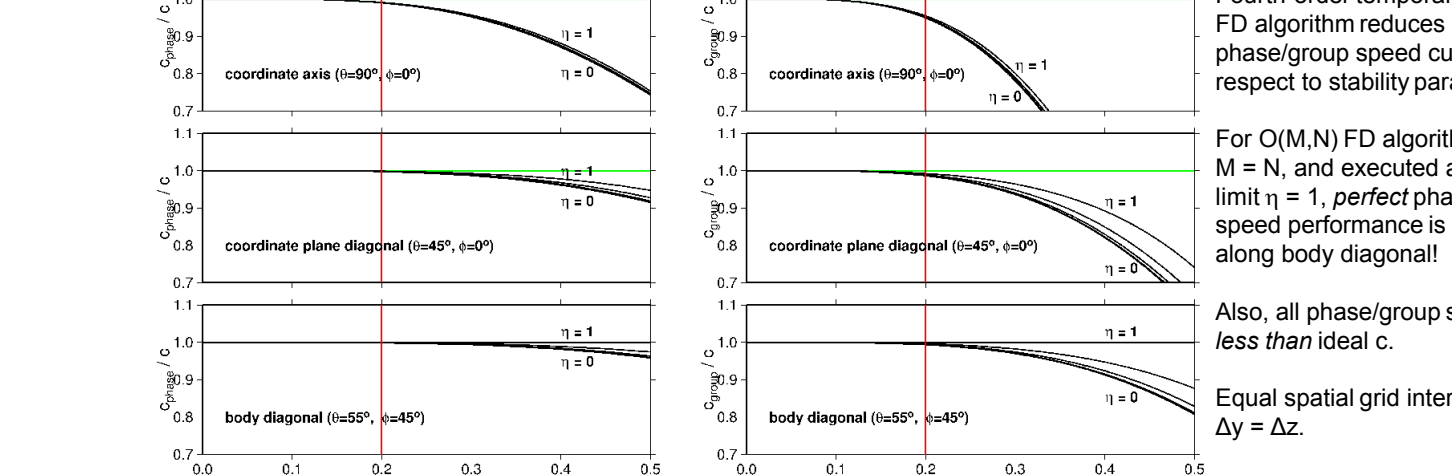


Crossline spatial grid interval Dy is four times larger than inplane spatial grid intervals $Dx = Az$.

Both in-plane and out-of-plane performance is adversely affected.

Extremely poor out-of-plane propagation performance.

O(4,4) Phase Speed



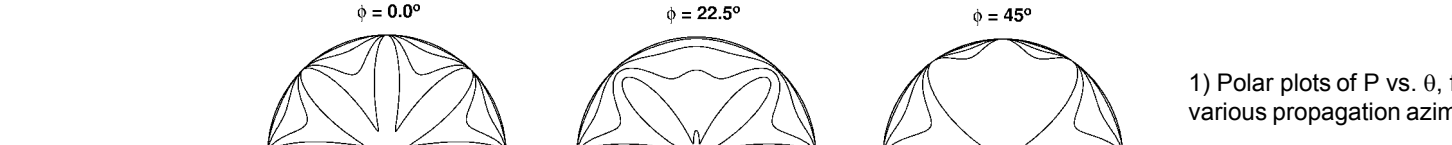
Fourth-order temporal operator FD algorithm reduces spread of phase/group speed curves with respect to stability parameter η .

For O(M,N) FD algorithms with $M = N$, and executed at stability limit $\eta = 1$, perfect phase/group speed performance is achieved along body diagonal!

Also, all phase/group speeds are less than ideal c.

Equal spatial grid intervals $\Delta x = \Delta y = \Delta z = \Delta \lambda$.

O(4,4) Group Speed

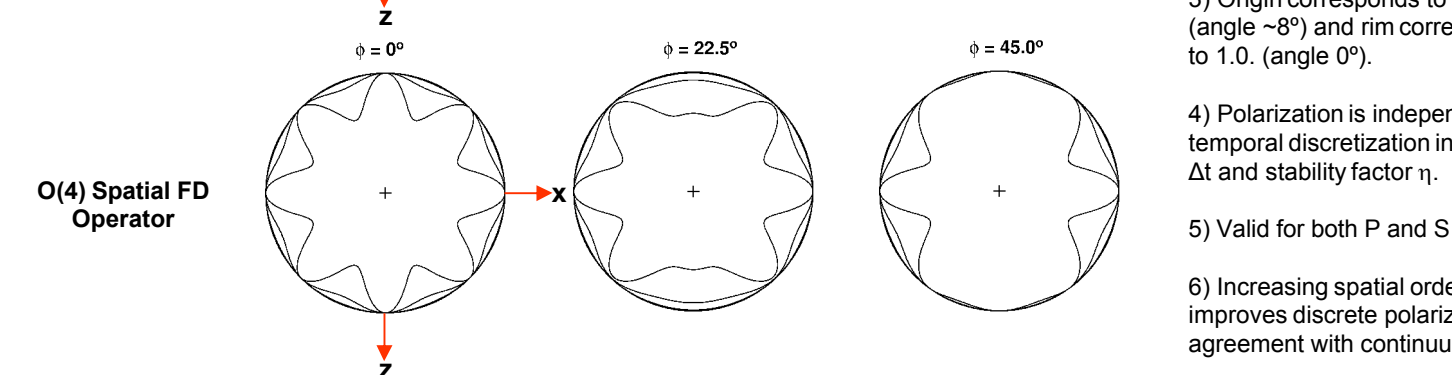


For O(M,N) FD algorithms with $M = N$, and executed at stability limit $\eta = 1$, perfect phase/group speed performance is achieved along body diagonal!

Also, all phase/group speeds are less than ideal c.

Equal spatial grid intervals $\Delta x = \Delta y = \Delta z = \Delta \lambda$.

Polarization vs. Plane Wave Propagation Direction



1) Polar plots of P vs. θ , for various propagation azimuths ϕ .

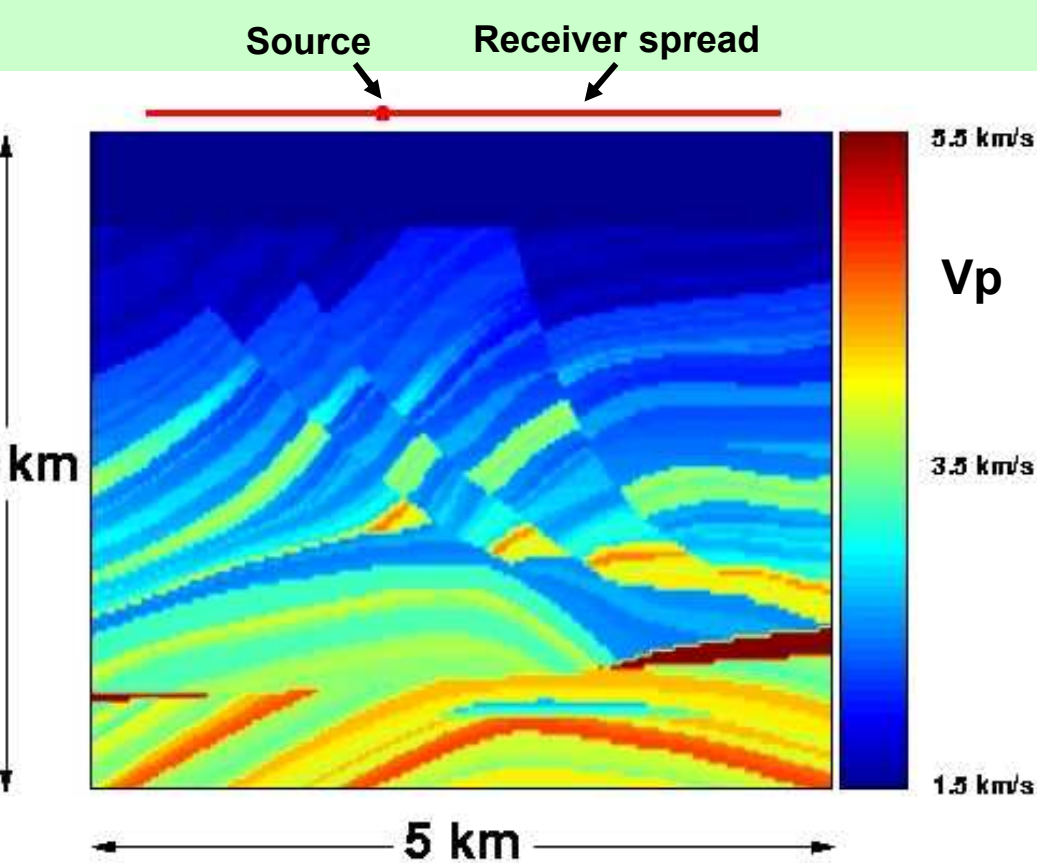
2) Each plot contains 6 curves, for spatial sampling ratio $s = 0$ (outermost curve) to 0.5 (innermost curve) in steps of 0.1.

3) Origin corresponds to 0.99 (angle ~8°) and rim corresponds to 1.0 (angle 0°).

4) Polarization is independent of temporal discretization interval Δt and stability factor η .

5) Valid for both P and S waves.

6) Increasing spatial order N improves polarization agreement with continuum case.



Numerical Dispersion Example: The Marmousi Model

The Marmousi model is a synthetic 2D earth model developed from geologic aspects of the Cuanza basin of offshore Angola. It contains several realistic features relevant to marine seismic exploration for petroleum: a water layer with a horizontal seabed, a sequence of dipping growth faults that offset and truncate sedimentary beds, anticlinal structures, two high-velocity salt sills, a near-horizontal erosional unconformity, and a deep petroleum reservoir. The model is commonly utilized to generate synthetic data for evaluating seismic reflection imaging algorithms. A 2D P-wave speed model, spatially sampled at $\Delta x = \Delta z = 24$ m, is obtainable at the website <http://www-rocq.inria.fr/~benamou/marmousi.html>.

We extrapolate the Marmousi model to three spatial dimensions, and calculate shot gathers and timeslices with a 3D O(2,4) FD algorithm based on the velocity-pressure equations of acoustic wave propagation. The required mass density model is generated via the Gardner relation $\rho = c V_p^{1/4}$.

Modeling Parameters:

- 1) Seismic source: isotropic explosion, 24 m deep, activated by a Ricker wavelet with 10 Hz peak frequency.
- 2) Seismic receivers: 341 hydrophones, 24 m beneath pressure-free surface of water layer, 12 m spacing.

Different spatial grid intervals are utilized in four FD simulations, in order to visualize and assess numerical dispersion effects in the calculated seismic data.

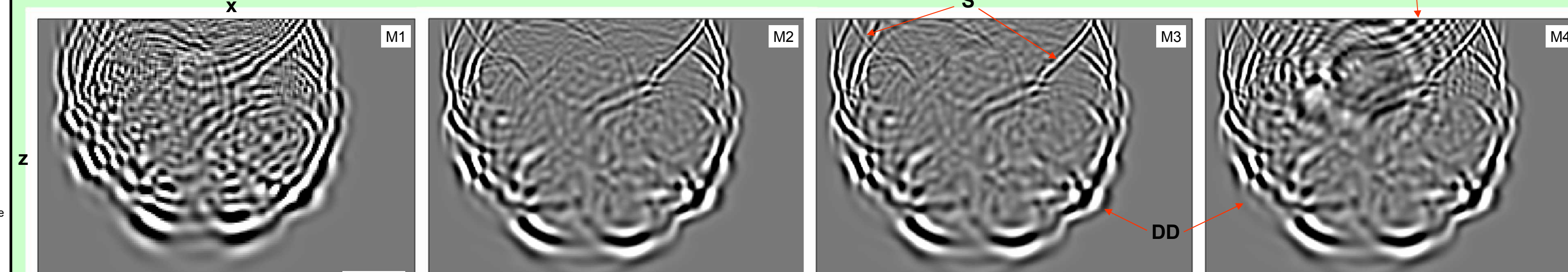
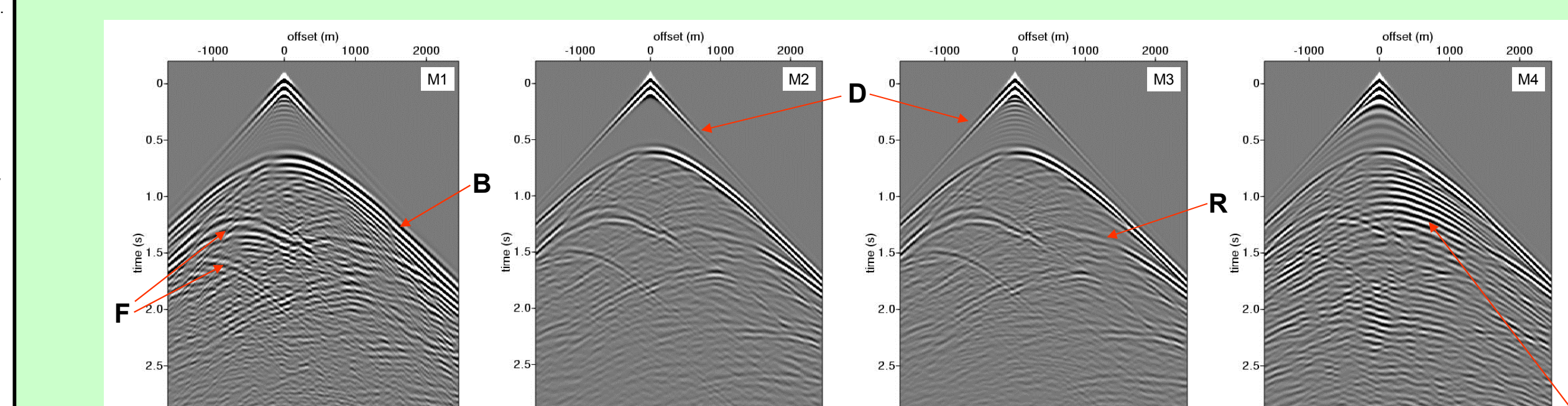
1) Note differences in direct wave (D), seabed reflection (B), sea-surface reflection (S), fault diffractions (F), and interface reflection (R).

2) Coarsely sampled model (M1, $\Delta h = 24$ m) and greatly enhanced crossline grid interval (M4, $\Delta y = 48$ m) generate dispersion noise.

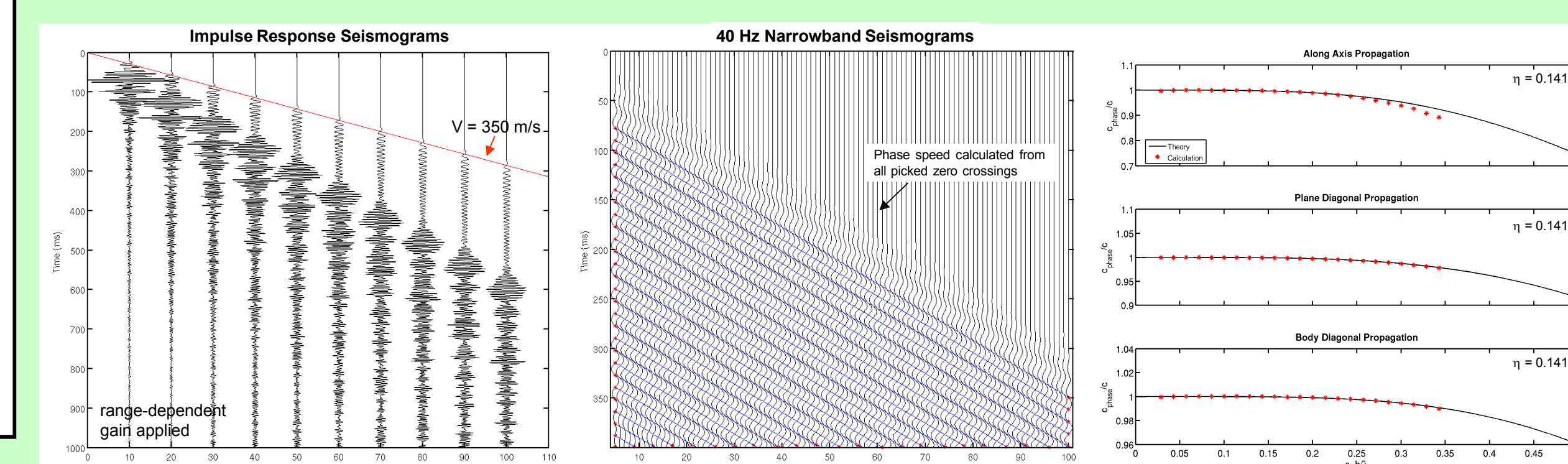
3) Finely sampled model (M2, $\Delta h = 12$ m) created by bilinear interpolation of download model (M1) appears superior, although M3 (with doubled Δy for rapid computation) is comparable.

4) Downgoing direct wave (DD) is very similar in models M2, M3, and M4.

Strong numerical dispersion noise!



Numerical Validation of Phase Speed Dispersion



Processing Procedure

1) Impulse response seismograms are generated by executing 3D FD algorithm with a unit impulse source waveform. Note severe numerical dispersion!

2) Impulse seismograms are convolved with a suite of narrowband signals, representing analogous harmonic source waveforms.

3) For each frequency, zero-crossings are picked, and phase speed calculated.

4) Example executes velocity-stress elastic algorithm with $V_p = 350$ m/s and $V_s = 0$ m/s (i.e., acoustic wave propagation example).